First-principles investigation of higher oxides of uranium and neptunium: U_3O_8 and Np_2O_5

Y. Yun,* J. Rusz, M.-T. Suzuki,† and P. M. Oppeneer
Department of Physics and Astronomy, Uppsala University, Box 516, SE-751 20 Uppsala, Sweden
(Received 14 September 2010; published 9 February 2011)

A computational study is presented of the structural, electronic, and magnetic properties of U_3O_8 and Np_2O_5, which are actinide oxides in a higher oxidation state than the tetravalent state of the common dioxide phases, UO_2 and NpO_2. The calculations are based on the density functional theory $+U$ approach, in which additional Coulomb correlations on the actinide atom are taken into account. The calculated properties of these two higher oxidized actinide oxides are analyzed and compared to those of their tetravalent analogs. The optimized structural parameters of these noncubic oxides are found to be in reasonable agreement with available experimental data. U_3O_8 is predicted to be a magnetic insulator, having one U atom in a hexavalent oxidation state and two U atoms in a pentavalent oxidation state. For Np_2O_5, which is also predicted to be an insulator, a complicated noncollinear magnetic structure is computed, leading to a nonzero overall magnetization with a slight antiferromagnetic canting. The calculated electronic structures are presented and the variation of the U $5f$ or Np $5f$–O $2p$ hybridization with the oxidation state is analyzed. With increasing oxygen content, the nearly localized $5f$ electrons of the actinide elements are more positioned near the Fermi level and the hybridization between $5f$ and $2p$ states is markedly increased.

DOI: 10.1103/PhysRevB.83.075109 PACS number(s): 71.28.+d, 71.20.−b

I. INTRODUCTION

Binary oxides of uranium and neptunium are very interesting materials, not only from a technological point of view as important constituents of the nuclear fuel cycle, but also from a scientific point of view as interestingly strongly correlated materials with a partially filled $5f$-electron shell. U and Np are known to exhibit various oxide phases with different oxidation states. The dioxides, UO_2 and NpO_2, are the most well-known stable oxide phases for both U and Np. UO_2 is a widely used nuclear fuel material. The electronic structure of UO_2 has been studied extensively using both experimental[1–6] and theoretical techniques.[4–13] Neptunium dioxide has recently attracted growing attention due to its complicated and mysterious magnetic multipolar ordering.[14–17] Both UO_2 and NpO_2 are, at elevated temperatures, paramagnetic and crystallize in the cubic fluorite structure, where each U or Np is surrounded by a cubic oxygen cage [see Fig. 1(a)]. Both dioxides exhibit a low-temperature phase transition. UO_2 undergoes a phase transition to an antiferromagnetic phase at 30.8 K accompanied by a lattice distortion.[18–20] The low-temperature properties of NpO_2 are more complicated than those of UO_2 and somewhat controversial. Especially the curious ordering phenomenon occurring below 25 K has attracted a lot of attention. Long-range magnetic ordering is absent in the low-temperature order state in spite of the $5f^3$ configuration of the tetravalent Np ion. Instead of the expected dipolar magnetic ordering, a second-order phase transition to a magnetic multipolar ordered phase occurs at low temperatures in NpO_2.[14–17]

Whereas most experimental and theoretical studies have focused on the dioxides, there is still quite a lack of knowledge on the higher U and Np oxides. The higher oxides have more complicated crystal structures compared to the dioxides and contain various inequivalent U-O or Np-O bonds. Some of the higher oxides crystallize even in several different crystallographic phases for the same chemical composition. Moreover, it is known to be very difficult to prepare single crystals of higher oxidized actinide compounds, because of the coexistence of various oxides with different oxidation states.[21] α-Triuranium octoxide, U_3O_8, is well known as one of several stable uranium oxides.[22,23] It is one of the essential materials in the nuclear industry because it is the major product of oxidation of UO_2 during fuel reprocessing or during long-term fuel storage.[24–27] The volume of U_3O_8 is increased by 38% relative to UO_2, which can lead to a breakdown of the fuel pellets into powder.[28–30] A similar hazard exists for long-term storage of spent nuclear fuel, as under oxidizing conditions UO_2 transforms to U_3O_8, which is actually the more stable binary uranium oxide.[29,30] At room temperature, α-U_3O_8 is paramagnetic and crystalizes in the orthorhombic crystal structure.[22,23] Its electronic structure has been investigated with x-ray photoelectron and x-ray-absorption spectroscopy[1,31–33] and electron-spin resonance.[34]

In contrast to the structural variety found for U, only two stable oxides have been found for neptunium, NpO_2 and Np_2O_5. Unfortunately, very little is known about the properties of Np_2O_5. Only recently, detailed crystal structure data of Np_2O_5 have become available; Np_2O_5 crystallizes in a monoclinic primitive cell and appears to order antiferromagnetically below 22 K.[35] Its volume is increased by 40% relative to that of NpO_2. The ordered magnetic moments on the Np ions in Np_2O_5 are not yet known.[35] Detailed electronic structure calculations for U_3O_8 and Np_2O_5 in their established crystal structures have not yet been reported. Pickard *et al.*[36] computed the optimized lattice parameters of hexagonal U_3O_8, which is the stable variant of U_3O_8 above 400 °C.[37] Furthermore, only several computational studies of the possible oxidation of actinide oxides through incorporation of additional interstitial oxygen atoms in the cubic dioxide lattice have been performed.[38–41]

Here we present computed electronic structure results for these uranium and neptunium oxides with a higher actinide oxidation state, using a density functional theory (DFT) based approach, supplemented with an additional on-site Coulomb U parameter on the actinide ions (so-called DFT + U method). The main part of this paper is devoted to providing a

first-principles based explanation of the electronic structures of the two higher oxides, α-U_3O_8 and Np_2O_5. In particular, we focus on the oxidation state of the actinide ions, the behavior of $5f$ electrons, and compare the electron density of states of $5f$ states and the $5f$–O $2p$ hybridization effects between the dioxides and the other higher oxides. Moreover, we compare the optimized structural properties to available experimental data. We also investigate the magnetic and metallic/insulating properties of all the oxides. The employed computational methodology is presented briefly in the next section. Subsequently, in Sec. III we present the computed results together with a detailed discussion.

II. COMPUTATIONAL METHODOLOGY

Our computational investigations have been performed using two different program packages, the VASP package,[42,43] which is a full-potential plane-wave code, in which pseudopotentials and the projector augmented wave (PAW) method are used, and the all-electron, full-potential linearized augmented plane-wave (FP-LAPW) code, in the WIEN2K implementation.[44]

To investigate the optimized crystal structures, we have employed the VASP code. A kinetic energy cutoff of 500 eV has been used for the plane waves in the basis set. The generalized gradient approximation (GGA) in Perdew-Wang '91 parametrization[45] of the exchange-correlation functional has been adopted, and, in order to treat electron correlations beyond those already included in the GGA, an additional Coulomb U on the actinide atoms was included (GGA + U method). The value of the Coulomb U has been varied in the range of 3–5 eV—which is the accepted range—using the $+U$ scheme of Dudarev and co-workers.[4–6] The exchange J was chosen to be 0.5 eV.

We have furthermore used the WIEN2K code[44] in two different versions for calculations of the electronic and magnetic structures. These are the standard WIEN2K (FP-LAPW) version for collinear magnetic systems as well as WIEN-NCM, the version for systems with noncollinear magnetism.[46] In the standard FP-LAPW calculations we employed the GGA Perdew-Burke-Ernzerhof (PBE)[47] exchange-correlation functional, but in the WIEN-NCM calculations we used the Perdew-Wang '92 local spin-density approximation (LSDA) parametrization.[48] In the FP-LAPW DFT + U calculations we used both the around mean-field (AMF)[49] and fully localized limit (FLL)[50] forms of the double counting term (for details of the $+U$ implementation in an FP-LAPW method, see Ref. 51). The self-consistent FP-LAPW DFT + U calculations have been performed including the spin-orbit coupling[52] and including semicore states.[53] We used for the Hubbard U parameter values ranging from 3 to 5.5 eV and for the exchange J values of 0.0 or 0.5 eV. We have determined the required number of k-mesh points from monitoring the saturated energy value of total-energy calculations performed for each system. For antiferromagnetic UO_2, $12 \times 12 \times 8$ k-points were used for the charge density integration within the Brillouin zone of the tetragonal unit cell. Paramagnetic NpO_2 has the conventional cubic fluorite unit cell, and the number of k points was increased up to $20 \times 20 \times 20$ points.

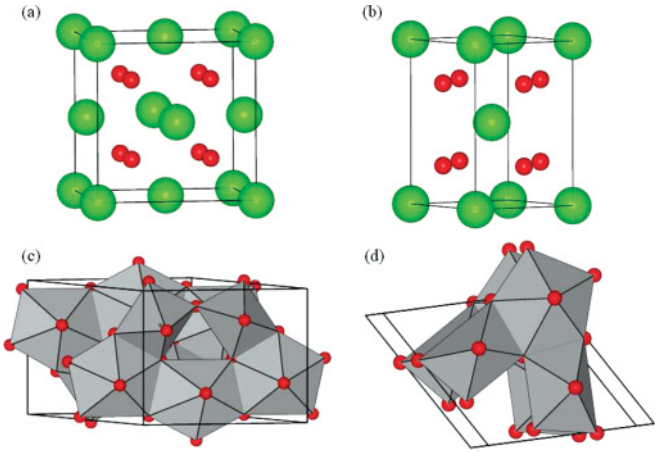

FIG. 1. (Color online) The crystallographic unit cells of (a) NpO_2, (b) UO_2, (c) Np_2O_5, and (d) U_3O_8. Green (large light gray) spheres depict Np or U atoms, the red (small dark gray) spheres show oxygen atoms.

For U_3O_8 and Np_2O_5, $6 \times 6 \times 9$ and $5 \times 6 \times 5$ k points were used, respectively.

III. RESULTS AND DISCUSSION

A. Crystal structures

Figure 1 shows the unit cells of the four actinide oxides. Both dioxides, NpO_2 and UO_2, crystalize in the cubic fluorite structure at elevated temperatures. NpO_2 stays in this cubic structure down to low temperatures, even though it undergoes a phase transition to a complex multipolar ordered state below 25 K.[54,55] Figure 1(a) shows the conventional cubic unit cell of NpO_2. UO_2 undergoes a phase transition to an antiferromagnetically ordered state below 30 K,[18,19] causing a symmetry breaking and a small tetragonal deformation.[20] For antiferromagnetic UO_2, we have used a double, tetragonal unit cell (with $c = \sqrt{2}a$) as shown in Fig. 1(b) where the magnetic ordering is along the [001] direction.[11,20] Figure 1(c) shows the unit cell of Np_2O_5, which has been determined[35] recently to be monoclinic with $\beta = 116.09^\circ$. There are four formula units in the monoclinic unit cell. The Np atoms form a chain consisting of two pentagonal bipyramids and one square bipyramid by sharing edges with adjacent pyramids. α-U_3O_8 has an orthorhombic structure,[22,23,26,28] built of three different pentagonal pyramids. The orthorhombic unit cell of U_3O_8, as shown in Fig. 1(d), has one formula unit per primitive cell. The atomic positions in the orthorhombic cell are such that the structure is close to a monoclinic primitive cell.

B. Charge densities

We start the presentation of our results with the computed electron charge density for the GGA + U optimized structures, which helps us to understand further the crystal structures and complex bonding of α-U_3O_8 and Np_2O_5.

Figure 2 shows the (FP-LAPW) GGA + U (PBE) computed charge density contour plot of Np_2O_5 in the $z = 0$ plane. The plotted charge densities pertain to the valence states only, summed over both spin directions; the electron density is indicated by the (logarithmic) color scale on the side. The

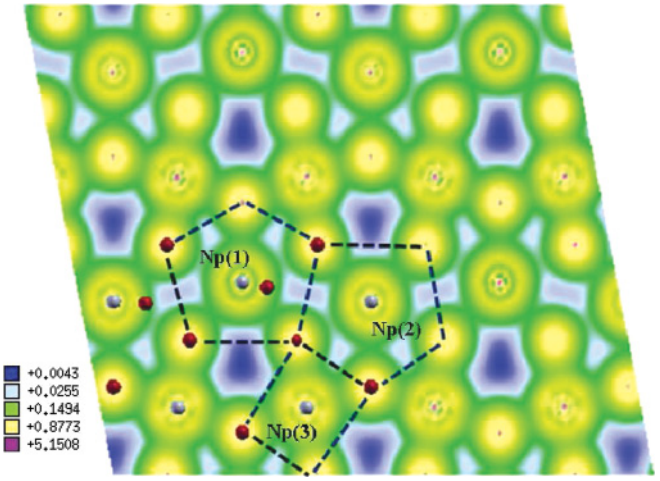

FIG. 2. (Color online) Contour plot of the GGA + U (U = 3.5 eV) calculated electron charge density of Np_2O_5 in the $z = 0$ plane. The three inequivalent Np atoms are located at the center of the dashed-line pentagons and rectangles. The red (dark gray) circles depict the O atoms.

unit cell of Np_2O_5 consists of two different kinds of pentagons and one rectangular structure, formed by the arrangement of Np and O atoms. The inequivalent Np atoms are located at the center of the two pentagons [denoted Np(1) and Np(2)] and the square [denoted Np(3)]; each of these Np atoms has a different distance to the nearest O atoms, which are 1.865, 1.885, and 1.958 Å, respectively. These distances are very short—less than 2.00 Å—approaching thus the possible limit according to the ionic radii of Np and O. The ionic radii of tetra-, penta-, and hexavalent Np ions are 1.01, 0.89, and 0.86 Å, respectively. The ionic radius of O^{2-} is known to be about 1.26 Å.[56] Hence the minimum distance between Np and O atoms is considered to be around 2.00 Å. Consequently, this suggests that Np_2O_5 could be the highest oxidized compound of Np.[56] This expectation is supported by the charge-density distribution in Fig. 2, too. The charge densities of Np and O atoms are located very close to one another and there is almost no interstitial region or low-density bridge region between Np and O atoms. If we compare to the (FP-LAPW) GGA + U computed electron charge density of U_3O_8, which is shown in Fig. 3 (bottom), we observe that some low-density interstitial region still exists between the central U atom and some of the O atoms in each pentagon (e.g., see the regions denoted by ① and ② in Fig. 3). This would imply that U_3O_8 could still be further oxidized. In fact, U_3O_8 has been found to be permeable to oxidation up to UO_3.[57,58]

The cross section of the crystal structure of α-U_3O_8 in Fig. 3 (top) illustrates that this uranium oxide also is built of pentagonal structures in the $z = 0$ plane. In the orthorhombic unit cell there are two equivalent U(2) atoms and one U(1) atom, and hence there are two different kinds of pentagons in the unit cell, related to the different distances between U and O atoms as indexed by ① and ② in Fig. 3 (top). Indices ① and ② label the distance between the central U and the most distant O atom in each pentagon; these distances are 2.54 and 2.72 Å in the two different pentagons, respectively. However,

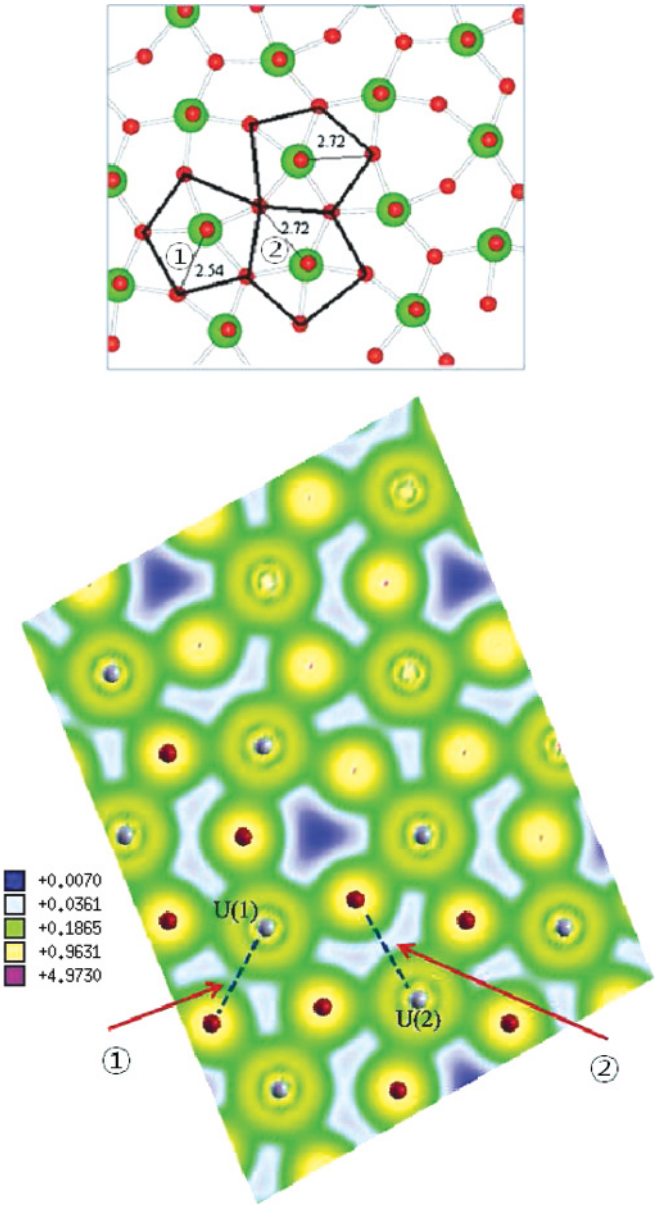

FIG. 3. (Color online) Top: Cross section of the unit cell of α-U_3O_8 in the basal plane, showing the pentagons of oxygen atoms surrounding the uranium atoms. Bottom: Contour plot of the GGA + U calculated electron charge density of U_3O_8 in the $z = 0$ plane (with U = 4.5 eV). The symbols ① and ② indicate the different distances between the central U atom and the most distant O atoms in the pentagons. The positions of the two inequivalent U atoms U(1) and U(2) are indicated in this panel.

the distances between the U's and the nearest O atoms are the same, 2.07 Å, for both pentagons.

C. Optimized structural data

In Table I we present the calculated structural data and available experimental data for the four oxides. The VASP-PAW approach was used for the structural optimization as this code is efficient for minimizing all atomic forces.[61] For the GGA + U (PW91) calculations presented in Table I, we have used U = 4.5 eV for the U atoms, a value that in

TABLE I. Calculated optimized structural properties of UO_2, U_3O_8, NpO_2, and Np_2O_5, compared with experimental data.[23,35,59,60] The Hubbard U energies used in the GGA + U calculations are 4.5 eV for U atoms and 3.5 eV for Np atoms, respectively.

		Lattice constant (Å)	
	Crystal structure	Expt.	Calc.
UO_2	cubic ($Fm\bar{3}m$)	5.47	5.51
		$a = 11.96$	$a = 11.61$
α-U_3O_8	orthorhombic ($C2mm$)	$b = 6.72$	$b = 7.20$
		$c = 4.14$	$c = 4.21$
NpO_2	cubic ($Fm\bar{3}m$)	5.43	5.42
		$a = 8.17$	$a = 8.28$
Np_2O_5	monoclinic ($P2c$)	$b = 6.58$	$b = 6.69$
		$c = 9.31$	$c = 9.46$
		$\beta = 116.09^\circ$	$\beta = 119.20^\circ$

previous studies[4–6] was determined through a comparison to experiment. For the Coulomb U on the Np atoms, we have investigated the effect of the adopted U parameter by calculating the electronic band gap and the magnetic moment for a range of effective U values, from $U_{\text{eff}} = U - J = 3$ to 5 eV. As will be discussed below, there is a sensitivity of the individual Np moments to the adopted U and J values, as well as to the double counting term used. The results listed in Table I are for $U = 3.5$ eV.

The computed equilibrium lattice parameters of the oxides, presented in Table I, are in reasonable agreement with the available experimental data.[23,35,59,60] UO_2 undergoes a small tetragonal distortion at low temperatures,[20] corresponding to a volume change of $\sim 10^{-5}$, but we have ignored this in our optimization, as the precise structural properties of UO_2 are not in the focus of the present study. The computed total moment per U atom is, with $1.69\mu_B$, close to the experimental moment of $1.74\mu_B$.[62] For NpO_2 we assume in this study a paramagnetic state, however, it is experimentally known to have a complex magnetic multipolar order below 25 K, with no or at the most a very small magnetic dipole moment.[63,64] This multipolar magnetic order of NpO_2 is a unique feature of this material, which has been found experimentally,[54,55] but is still not well understood. We have chosen here to treat NpO_2 in the paramagnetic state, with the aim to come as close as possible to its magnetic ground state having no ordered dipolar moment. Even in spite of this approximation, our computed lattice parameter of NpO_2 agrees well with the experiment.[60] A recent GGA + U structural optimization, which, in contrast to our calculations, did not include the spin-orbit interaction, obtained a smaller lattice constant of 5.40 Å.[65] It is known that the inclusion of spin-orbit interaction in the structural optimization of actinide compounds leads to larger equilibrium lattice constants.[52] We note, however, that while the inclusion of a Coulomb U normally leads to the increase of a gap for typical Mott-Hubbard insulators, we find here that nonmagnetic GGA + U calculations *fail* to explain the opening of a gap; also GGA calculations cannot explain the insulating state. A precise value of the excitation gap in the magnetic multipolar state is not known, but it is estimated to be larger than 0.4 eV,[64] and to be comparable[66] to the gap in antiferromagnetic UO_2.[67] The Np ions in cubic NpO_2 are expected to be in a tetravalent $5f^3$ configuration that normally should sustain a magnetic, metallic state.

The optimized lattice parameters of U_3O_8 and also Np_2O_5 deviate more (about 6%) from the experimental data than those computed for the dioxides (about 2%). The deviation appears to be largest for U_3O_8. It is not clear what the origin of this difference is. A deviation of the oxygen stoichiometry in the higher actinide oxides might have some influence on the experimental data. Noteworthy, a previous investigation[36] of *hexagonal* U_3O_8, using the LDA exchange-correlation parametrization without additional Coulomb U and neglecting the spin-orbit interaction achieved quite good agreement with experiment for the structural parameters. Although we do not investigate the high-temperature hexagonal phase of U_3O_8 here, we have tested the performance of the GGA (PW91) functional for the optimization of orthorhombic U_3O_8. We obtained $a = 11.85$ Å, $b = 6.81$ Å, and $c = 4.16$ Å. These values are closer to the experimental data than those obtained from optimization on the GGA + U level. A reason for the better performance of the GGA optimization is not evident. It is to be expected that the Coulomb U and also spin-orbit interaction should play a role to achieve an appropriate electronic structure. In particular, for uranium dioxide the additional Coulomb U must be included to achieve agreement with experiment for electronic structure properties such as the band gap and magnetic moments. However, in contrast to LDA or GGA calculations the $+U$ calculations might be affected by convergence to a metastable state. We can safely exclude this possibility For UO_2 and NpO_2, because for these materials convergence to the overall ground state is readily obtained. For Np_2O_5 we have performed many different $+U$ calculations, but always converged to a similar ground state, which is a strong indication that a metastable state can be excluded for Np_2O_5 as well. We can, however, not completely exclude the existence of a metastable state for U_3O_8. It deserves, furthermore, be noted that the GGA + U structural optimization for Np_2O_3 provided results in better agreement with the experimental data,[35] also for the internal atomic positions. To describe the electronic structures of U_3O_8 and Np_2O_5 as accurately as possible we have adopted the experimental coordinates in the following.

D. Computed electronic properties of U_3O_8

The electronic and magnetic properties of orthorhombic U_3O_8 to be discussed below have been computed with the FP-LAPW GGA + U approach, using the experimental coordinates. To start with, we mention that calculations for UO_2 have shown that the VASP-PAW and FP-LAPW approaches provide very similar electronic structures. The partial DOS of antiferromagnetic UO_2, computed with VASP-PAW (see Ref. 11) is very similar to the FP-LAPW partial DOS shown in Fig. 4. We turn now to U_3O_8. The magnetic properties of U_3O_8 have not yet been investigated in detail. Several experiments reported that α-U_3O_8 has a paramagnetic state at room temperature.[23,28] Our (FP-LAPW) GGA + U (PBE) calculations predict that α-U_3O_8 should have a magnetic ground state at $T = 0$ K. A simple consideration of the valency of uranium in α-U_3O_8 indicates that two U ions could be

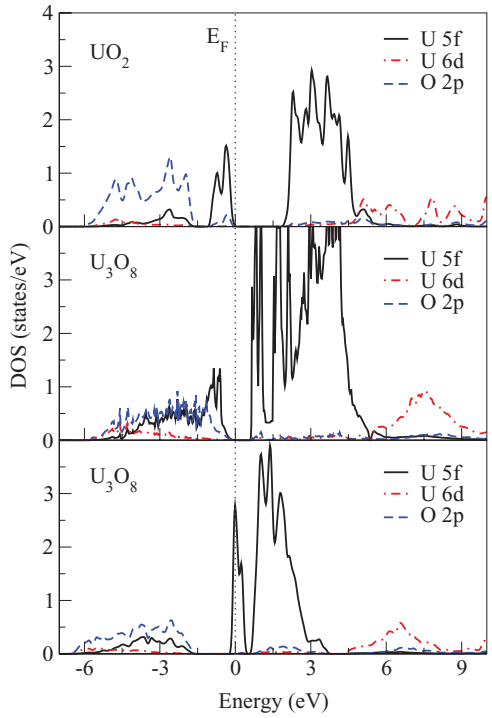

FIG. 4. (Color online) Calculated GGA + U partial DOS of UO_2 (top panel), ferromagnetic U_3O_8 (middle panel), and of paramagnetic U_3O_8 (bottom panel), for $U = 4.5$ eV.

hexavalent and one U ion tetravalent, or, alternatively, two U ions could be pentavalent and one U ion hexavalent. Thus either one or two of the three uranium atoms would be magnetic. As discussed in more detail below, our GGA + U and LSDA + U calculations predict the latter case, i.e., that one U atom is hexavalent. We obtained the minimal total energy of α-U_3O_8 for a ferromagnetic state with a total magnetic moment of $0.74\mu_B/U_3O_8$. This magnetically ordered state has a deeper total energy (by about 1.5 eV) than the nonmagnetic state. We have furthermore checked the stability of the magnetic phase of U_3O_8 by decreasing the Coulomb U from 4.5 to 0 eV. We found that the ferromagnetic state remains stable, having the deepest total energy regardless of the U value. The relatively small total magnetic moment of U_3O_8 derives from the difference of the orbital and spin moment of $5f$ electrons, which are antiparallel to each other, as presented in Table II. Counting also the spin moment on the oxygen atoms and in the interstitial space, we obtain a total spin moment of $0.98\mu_B$. Uranium atoms in the second position contribute also with an antiparallel orbital moment of $1.72\mu_B$ per formula unit. Both orbital and spin moments are calculated to be much smaller in U_3O_8 than in UO_2. This variation of the local magnetism on the U atoms is obviously related to the $5f$ oxidation, which is associated with the configuration of nearest-neighbor (NN) O atoms. Comparing these distances in UO_2 and U_3O_8, we see that the nearest-neighbor distance between U and O atoms is about 13% shortened, from 2.37 Å in UO_2 to 2.07 Å in U_3O_8. This leads to the increased hybridization of U $5f$ and O $2p$ states, a higher oxidation of the U atoms, and hence a decrease of the magnetic moment. One of the U atoms in the unit cell, U(1), is predicted to have completely no magnetic

TABLE II. Calculated magnetic moment (in μ_B) of the two inequivalent U atoms in U_3O_8, indexed U(1) and U(2), which have multiplicity 1 and 2, respectively. M_L and M_S are the orbital and antiparallel spin moment, respectively, and M_{tot} is the total magnetic moment of each U atom, along the c axis.

	M_L	M_S	M_{tot}
U(1)	0.00	0.00	0.00
U(2)	−0.86	0.45	0.41

moment, which could imply that this U ion corresponds to a highly oxidized, $5f^0$ hexavalent state. This point of view is supported by the configuration of the NN O atoms surrounding the U(1) atom. The seven NN O atoms of U(1) are in a very symmetric configuration, in which three pairs of O atoms are located at opposite directions to one another with regard to the U(1) in the center, and their distances to the U(1) atom are exactly the same (see Ref. 23). The distances of the oxygen atoms in the polygons surrounding the central U atoms are summarized in Table III for convenience. Except for the first NN O pair positioned at the pyramid's apex in the $\pm z$ directions as 2.07 Å [see Fig. 1(d)], the other NN O atoms are located in the plane of the pentagonal structure ($z = 0$ plane, see Fig. 3). The spin moment on U(2) is $0.45\mu_B$ (see Table II), and the total spin moment of the cell is nearly $1\mu_B$. These values are moderately consistent with the Hund's rules for a $5f^1$ configuration. The spin moment on U(2) is reduced from the maximal Hund's rule value of $1\mu_B$. This can be due to the effects of the relativistic spin-orbit interaction beyond Russell-Saunders coupling. The orbital moment on U(2) appears to be quenched through the crystal field. The configuration of the seven NN O atoms surrounding the U(2) atom in the pentagon's plane is not symmetric, as each of the O atoms has a slightly different distance to the U(2). In particular, there is one O atom that has a much longer distance (of 2.72 Å) to the U(2) atom (see Table III). For the U(1) atom the longest U-O distance is 2.54 Å. Hence these data also support the view that the U(2) atom is not as highly oxidized as the U(1) atom. We mention that the uranium valencies in U_3O_8 have been controversially discussed in the literature. X-ray photoemission spectroscopy (XPS) measurements on UO_2, U_3O_8, and UO_3 have been interpreted as evidence for the presence of one tetravalent and two hexavalent U atoms.[1,31,32] Electron spin resonance (ESR) measurements, on the other hand, have been interpreted as evidence for a configuration consisting of one hexavalent and two pentavalent U atoms.[34]

From our calculations we obtain that α-U_3O_8 has a magnetic ground state which corresponds to one nonmagnetic, i.e., suggesting hexavalent U atom and two relatively weakly magnetic, possibly pentavalent, U atoms per formula unit. The computed magnetic order is ferromagnetic. We mention that we have tried to obtain a symmetry-broken, antiferromagnetic coupling between the two U atoms, however, within the self-consistent cycle the antiferromagnetic state converged to a ferromagnetic state. Nonetheless, it cannot be fully excluded that a more complex antiferromagnetic order exists. Earlier experiments found no indication of magnetism in α-U_3O_8 at room temperature,[23,28] which would suggest the existence of a possible Néel or Curie point at lower temperatures. We propose

TABLE III. Distances (in Å) of the surrounding nearest-neighboring oxygen atoms to the two inequivalent uranium ions in U_3O_8 and the three inequivalent Np ions in Np_2O_5, respectively.

Oxygen	U(1)	U(2)	Np(1)	Np(2)	Np(3)
1st NN O	2.07	2.07	1.87	1.89	1.96
2nd NN O	2.07	2.07	1.87	1.89	1.97
3rd NN O	2.16	2.13	2.29	2.35	2.13
4th NN O	2.16	2.15	2.41	2.35	2.16
5th NN O	2.26	2.18	2.41	2.44	2.31
6th NN O	2.26	2.21	2.60	2.60	2.35
7th NN O	2.54	2.72	2.60	2.60	

that low-temperature experiments on single-crystalline α-U_3O_8 could shed light on this issue.

To compare further the hybridization between the U $5f$ and oxygen $2p$ states in UO_2 and α-U_3O_8, we have calculated their partial density of states (DOS). In Fig. 4 we show the DOS of UO_2 and of ferromagnetic and paramagnetic U_3O_8. Both antiferromagnetic UO_2 and ferromagnetic U_3O_8 are calculated to be insulators with energy band gaps of 1.84 eV and 0.50–0.63 eV (depending on $+U$ parameters and double counting form, respectively). The computed energy gap of UO_2 is in good agreement with experiment (2.0 eV),[67] but no data are available for U_3O_8. Paramagnetic U_3O_8, however, is computed to be metallic, due to a very narrow $5f$ band that becomes pinned at the Fermi energy (E_F). Figure 4 shows that the valence bands are dominated by O $2p$ and U $5f$ states both in UO_2 and U_3O_8. In both compounds there is a clear U $5f$–O $2p$ hybridization, as can be recognized from the coinciding peak positions in the partial DOS below E_F. From UO_2 to U_3O_8 a strong increase of the U $5f$ partial DOS is clearly visible in the energy range of -6 to 0 eV, and the peaks of U $5f$ DOS coincide with those of the O p states. This shows a significantly increased hybridization between U $5f$ and O $2p$ states in U_3O_8. The U $6d$ states, conversely, are not notably changed through further oxidation of the uranium dioxide. Figure 4 furthermore illustrates that the exchange splitting of the uranium $5f$ orbitals is responsible for the formation of the energy gap. In the ferromagnetic phase there is a majority spin peak 0.8 eV below E_F and also a sharp peak at 0.7 eV above E_F. In the paramagnetic phase, these two peaks collapse to one peak which is—due to its filling—pinned at the Fermi level. As a result of the exchange splitting, the $5f$ partial DOS of U_3O_8 above E_F is broader in the ferromagnetic than in the paramagnetic phase. We mention furthermore that the computed DOS of magnetic U_3O_8 is in reasonable agreement with XPS experiments.[68] XPS measurements[68] indicate a $5f$ peak between 0 and 2 eV binding energy, which would correspond to the computed $5f$ intensity at about -1 eV. The measurements also reveal an oxygen dominated broad hump in the XPS extending from 2 to 8 eV binding energy, also seen in x-ray emission experiments.[33] This corresponds to the computed O $2p$ partial DOS, which, however, extends only to -6 eV in the calculations.

To clarify further the electronic structure of α-U_3O_8 we show in Fig. 5 the computed energy-band dispersions along the high-symmetry points Γ-Y-Δ_0-Γ-Z-T-B_0-Z, in the orthorhombic Brillouin zone (BZ). In addition we highlight the

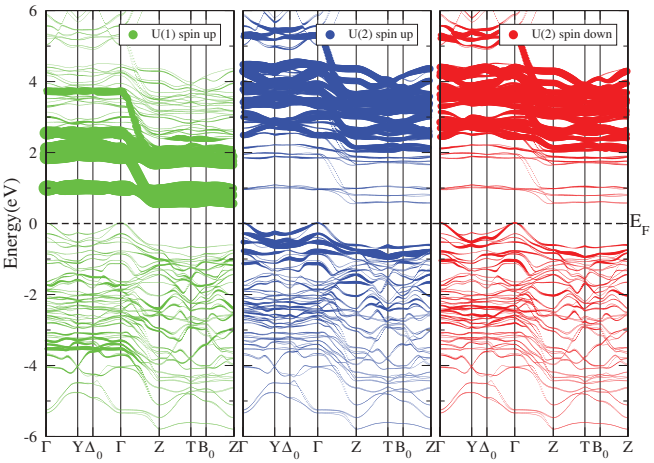

FIG. 5. (Color online) Calculated energy-band structure of magnetic U_3O_8 along the high-symmetry directions of the orthorhombic Brillouin zone. The special points are defined by $\Gamma = (0,0,0)$, $Y = (1,0,0)$, $\Delta_0 = (1,u,0)$, $Z = (0,0,\frac{1}{2})$, $T = (1,0,\frac{1}{2})$, and $B_0 = (1,u,\frac{1}{2})$ [with $u = 1 + (a^2 - b^2)/ab$]. The three panels highlight through the fatness of the bands the amount of spin-polarized $5f$ character in the energy dispersions that is due to the inequivalent U(1) and U(2) atoms. For the nonmagnetic U(1) atom only the spin-up projection is shown as spin-up and -down contributions are identical.

amount of spin- and atom-projected $5f$ character in the energy bands through the fatness of the bands, separately for the U(1) and U(2) atoms. At the bottom of the conduction band, at 1 and 2 eV, there are several flat bands that are nearly dispersionless throughout the BZ, except for some dispersion along Γ-Z. The fatness character shows that these bands are due to the U(1) $5f$ states, which, in this energy interval, practically do not hybridize with unoccupied O $2p$ states. Below E_F there is practically only a contribution from the U(2) spin-majority $5f$ states, which hybridize strongly with the oxygen p states between E_F and 2 eV below. Unoccupied $5f$ states of the U(2) atom appear again 2.5 eV above E_F.

E. Computed electronic properties of Np_2O_5

We now turn to Np_2O_5. The calculated crystallographic results for Np_2O_5 agree reasonably well with the recent experimental data;[35] see Table I. Calculating the total energy of Np_2O_5 for different magnetic configurations, we find that an overall ferromagnetically ordered state is the most stable one for Np_2O_5. Magnetic ordering is in itself in accordance with experiment,[35] in which magnetic order was concluded from a maximum in the temperature-dependent susceptibility at 22 K. However, the drop of the susceptibility below 22 K suggested antiferromagnetic Np-Np interactions.[35] Our initial calculations assuming a collinear magnetic structure indicated strong spin-off–diagonal components due to strong spin-orbital interaction, which predicted a deflection of the orbital moment from the spin quantization axis. Hence we performed subsequent noncollinear magnetic calculations, testing both AMF and FLL variants of the LSDA + U (PW92) approach and varying the U value between 3 and 5.5 eV, and the J value was set to 0.0 or 0.5 eV. The resulting noncollinear magnetic structure is depicted in Fig. 6. It leads to a net ferromagnetic

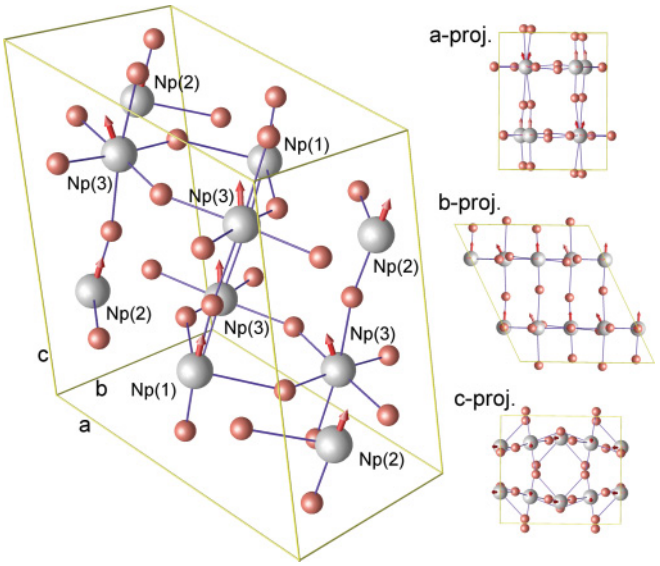

FIG. 6. (Color online) The LSDA + U computed noncollinear magnetic structure of Np_2O_5 and its projections along the a,b, and c monoclinic unit-cell axes.

moment approximately along the c axis and in addition it has a weak antiferromagnetic component within the a-b plane.

A summary of the calculated magnetic moments is presented in Table IV (for the sake of brevity not all calculated variants are listed). Generally, calculations with the same effective $U_{\text{eff}} = U - J$ give very similar magnetic moments—typically calculations with zero J enhance the magnetic moments by less than $0.1\mu_B$. The only notable exception is a FLL calculation with effective $U = 3$ eV, where the magnetism on the Np(3) sublattice becomes more strongly enhanced at zero J. The change of moments with different values of U is found to be surprisingly weak in these calculations, the moments even slightly decrease with increased U. This, and the presence of strongly reduced moments on the Np(3) site, indicates some sort of frustration of the magnetic structure, which gets more pronounced with increased localization of $5f$ electrons (i.e., with larger U value). The here-suggested magnetic frustration is consistent with experiment, in which competing exchange interactions were deduced from the measured susceptibility.[35] The magnetic order in Np-O compounds appears to depend sensitively on the Np-O-Np superexchange pathways. Both antiferromagnetic[69] and ferromagnetic[70–72] orders have been found in Np(V) oxide complexes, as well as paramagnetic complexes,[73] but ferromagnetic order generally dominates.[70]

By far the largest difference in the computed moments stems from the different LSDA + U double counting variants. In FLL calculations the spin magnetic moments become substantially enhanced (by approximately $0.5\mu_B$). The orbital moments are also enhanced, but by a smaller amount. As the orbital moments are oriented in opposite directions, this implies a net decrease of the total magnetic moment per formula unit in the FLL calculation. The total magnetic moment varies, depending on the LSDA + U variant and used parameters, between $2.4\mu_B$ and $2.8\mu_B$. An experimental value is presently not available.

We have also calculated the band gap as a function of U. The computed energy band gap varies from 1.8 to 2.7 eV, depending on the double counting variant and parameters of the $+U$ scheme (generally, the gap size increases with U_{eff}, and also FLL leads to wider gaps than AMF). We mention that from the available results it is not yet possible to extract the applicable value of U. An effective U value of 3 eV provides good agreement with experiment for the crystal structure, but it is not yet obvious why the U value would be smaller than for the uranium oxides. At present there is not yet a sufficient body of experimental data for the Np oxides available to compare with the computed properties.

From a simple valency consideration one would expect all Np ions in Np_2O_5 to be in the pentavalent $5f^2$ state. Due to the complex crystal structure, however, there are some distinct differences between the three inequivalent Np ions. Table IV illustrates that the on-site Np spin moments of the first two inequivalent Np atoms are nearly the same, while the magnetism is strongly suppressed on the third Np atom position, hence this atom (which has a multiplicity of 4) contributes dominantly to the lowering of the total magnetic moment of Np_2O_5. The similarity of the Np(1) and Np(2) moments can be traced back to their rather similar Np-O coordination of seven NN oxygens in similar pentagonal bipyramids (see Fig. 2), with comparable average Np-O distances (see Table III). The Np(3) ion, however, has six NN oxygens and is located in a square bipyramid of four oxygen atoms in the $z = 0$ plane having an averaged Np-O bond length shorter than that in the pentagonal bipyramids (Fig. 2). Hence the Np-O bonding as well as crystal field is different for

TABLE IV. Calculated magnitudes of spin (M_S), orbital (M_L), and total (M_{tot}) magnetic moments in μ_B of the three inequivalent Np ions in Np_2O_5, as a function of the U and J parameters, as well as the variant of the LSDA + U scheme.

Method	LSDA + U parameters (eV)	M_S			M_L			M_{tot}
		Np(1)	Np(2)	Np(3)	Np(1)	Np(2)	Np(3)	f.u.
AMF	$U = 3.0$, $J = 0.0$	1.22	1.19	0.17	−4.01	−3.88	−0.15	2.63
AMF	$U = 3.5$, $J = 0.5$	1.21	1.18	0.09	−4.08	−4.02	−0.03	2.69
AMF	$U = 5.0$, $J = 0.0$	0.97	0.94	0.06	−3.94	−3.83	−0.04	2.80
AMF	$U = 5.5$, $J = 0.5$	1.01	0.98	0.06	−4.03	−3.94	−0.01	2.82
FLL	$U = 3.0$, $J = 0.0$	1.68	1.67	0.75	−4.16	−4.13	−0.76	2.44
FLL	$U = 3.5$, $J = 0.5$	1.59	1.57	0.17	−4.24	−4.22	−0.09	2.54
FLL	$U = 5.0$, $J = 0.0$	1.67	1.67	0.38	−4.26	−4.21	−0.39	2.56
FLL	$U = 5.5$, $J = 0.5$	1.59	1.58	0.14	−4.30	−4.27	−0.09	2.63

the Np(3) ion. The NN distances of the six oxygens to the Np(3) ion are more similar, whereas the distances of the seven surrounding NN oxygens are more spread out for Np(1) and Np(2); see Table III. This suggests that the oxygen surrounding of Np(3) might lead to a larger crystal-field quenching of the orbital moment on Np(3). Alternatively, the smaller moment on Np(3) could be attributed to a different oxygen bonding or to some influence of the magnetic frustration on the system. The occurrence of relatively large moments on the Np(1) and Np(2) ions appears to be compatible with a pentavalent $5f$ configuration, which, according to Hund's rules for free atoms, would have a $2\mu_B$ spin moment and $-5\mu_B$ orbital moment. The computed moments in Table IV are, however, reduced from these theoretical values. The Np(3) ion could also have a pentavalent configuration, but be affected by a different bonding and crystal field. As mentioned above, the latter is more cubic. By looking at the number of $5f$ electrons in the muffin-tin spheres, we obtain a similar amount of electrons for all Np positions and all U and J combinations, although Np(3) has systematically 0.1 f electron less compared to Np(1) and Np(2). Nonetheless, this suggests a pentavalent configuration for the Np(3) ion, too.

The computed partial DOSs of the two Np oxides are shown in Fig. 7. The presented DOS was obtained by using a Coulomb U of 3.5 eV in GGA + U calculations. Paramagnetic NpO_2 is predicted to be metallic, whereas magnetic Np_2O_5 is predicted to be an insulator with a band gap of about 2 eV. Experimentally, NpO_2 in the magnetic multipolar ordered state is an insulator, but paramagnetic single-particle DFT + U calculations fail to capture this complex many-electron behavior. The Np ion in NpO_2 has a $5f^3$ configuration, which, according to Hund's rules, should prefer a $3\mu_B$ spin moment, but experimentally it is known that this does not happen, rather, a magnetic multipolar state is formed.[15–17] When a paramagnetic solution is enforced in GGA + U calculations, NpO_2 must become metallic, due to the incomplete $5f$ state filling. It has been shown recently that, assuming an ordered large-moment antiferromagnetic configuration for NpO_2, an insulator state can be obtained,[10,65] but the large ordered moment on the Np is in contradiction with experiment.[55,63] Another recent investigation showed that the formation of a triple-$\boldsymbol{k}$ magnetic multipole ordered state indeed leads to the opening of a respectable band gap.[74] The computed DOS of *nonmagnetic* NpO_2 in Fig. 7, however, consists of an unhybridized narrow Np $5f$ band positioned at the Fermi level. At higher binding energies of 3–6 eV, there is a manifold of hybridized O $2p$ and Np $5f$ states. Comparing the partial DOS of Np_2O_5 to that of NpO_2, it can be recognized that the intensity of the Np $5f$ contribution in the manifold of occupied states becomes clearly enhanced for Np_2O_5, which implies a marked increased Np $5f$–O $2p$ hybridization. The possibility of a strong Np-O hybridization in Np_2O_5 has been considered recently. Forbes *et al.*[35] observed that the experimental effective moment in the paramagnetic regime is, with $2.2\mu_B$, substantially smaller than the Np^{5+} free ion value of $3.58\mu_B$. This was attributed to an amount of delocalization of the Np $5f$ electrons due to strong oxygen $2p$ bonding or to a quenching of the orbital moments by the crystal field.[35] Our above discussion pinpoints a mixing of these two effects. A strong oxygen bonding is present for all three Np ions, causing an amount of delocalization of the $5f$ electrons. The larger contribution to the reduction of the total moment stems, however, from the crystal-field quenching on Np(3), which, with its multiplicity of 4, contributes markedly to the reduction of the moment. A change in Np-O bonding with oxygen stoichiometry has also been observed in recent ultraviolet photoemission spectroscopy (UPS) measurements of oxidized Np surfaces.[75] In these experiments the reaction of a Np surface with oxygen was studied under variation of the oxygen concentration and the energy positions of the O p and Np f electronic densities were determined with UPS. Although the crystalline structure of the oxide layers cannot be accurately determined, UPS for a Np : O composition of 1 : 2 shows a separated oxygen and neptunium response, at -8 to -3 eV, respectively, -3 to -1 eV. These energies correspond to the partial DOSs of NpO_2 in Fig. 7, except that in the calculation the Np $5f$ are shifted more toward E_F. Upon oxidation the oxygen and neptunium UPS responses shift and merge.[75] The oxygen DOS from an oxidized surface (expected to have a close to 2 : 5 stoichiometry) extends from -7 to -1 eV, whereas the $5f$ response appears dominantly between -2 and -1 eV. In Fig. 7 a similar energy shift in the O p DOS and merging with the Np $5f$ states is visible in the computed DOS. Figure 7 furthermore illustrates that the conduction bands in both Np oxides, which are mainly due to unhybridized Np $5f$, do not change much, apart from a widening of the unoccupied $5f$ states being again due to the exchange splitting in Np_2O_5. A confirmation of the existence of a band gap in magnetically ordered Np_2O_5 does not yet exist. Experimental investigations of the temperature-dependent resistivity of Np_2O_5 would hence be a definite test of the predicted insulating state.

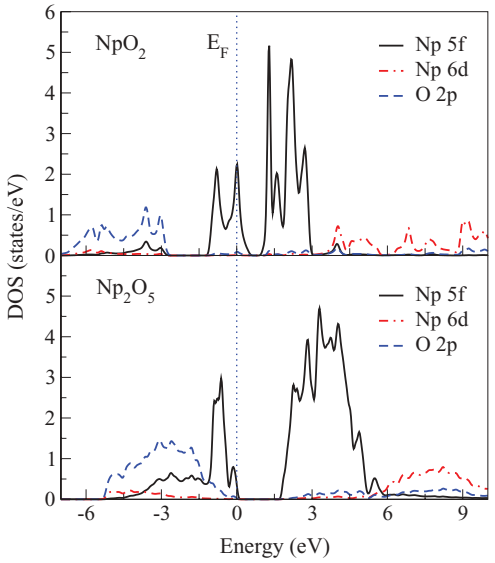

FIG. 7. (Color online) Calculated GGA + U partial DOS of paramagnetic NpO_2 (top panel) and ferromagnetic Np_2O_5 (bottom panel) for $U = 3.5$ eV.

IV. CONCLUSIONS

We have performed DFT + U electronic structure investigations of α-U_3O_8 and Np_2O_5. The structural parameters of these actinide oxides, as well as of the tetravalent actinide oxides UO_2 and NpO_2, have been studied through total-energy

optimization. The calculated structural parameters are found to agree reasonably well with experimental data. Both U_3O_8 and Np_2O_5 are predicted to be magnetic insulators in the ground state. Our calculations suggest that in U_3O_8 one of the inequivalent U atoms is in a hexavalent oxidation state, and the other two U atoms are in a pentavalent oxidation state. For Np_2O_5 our calculations reveal differences between the three inequivalent Np ions, due to differences in the nearest-neighboring oxygen surrounding. The valencies of the Np ions are nonetheless expected to be identical. Inspection of the computed electron density of Np_2O_5 reveals that, due to a close packing of Np and O atoms, there is not much low-density region available. This indicates that pentavalent Np is the highest known oxidation state for Np in a neptunium oxide. It can, however, not be excluded that further oxidation might occur at the surface of Np_2O_5, similar to what has possibly happened for PuO_2 (see, e.g., Ref. 76). Comparing to α-U_3O_8, its computed electron-density map contains more low-density regions between the U and O atoms, indicating that U_3O_8 can be further oxidized, which is in accord with experimental observations.[57,58]

U_3O_8 is predicted to order ferromagnetically, whereas for Np_2O_5 our calculations predict noncollinear magnetic order, with a ferromagnetic exchange coupling along the c axis and a weaker antiferromagnetic coupling in the a-b plane. The latter system is observed to exhibit some magnetic frustration, within the asymmetrically connected Np-O network. Connected to this is that we find the calculated magnetic moments in Np_2O_5 to be rather sensitive to the used Hubbard U parameter as well as to the form of the $+U$ double counting term.

A comparison of the hybridization of the actinide $5f$ states with oxygen $2p$ states in the higher oxides with that of the dioxides reveals a much enhanced hybridization. The actinide $5f$ electron density is spread throughout the O $2p$ density in the valence band, whereas in the actinide dioxides the $5f$ density is much more disjunct from the O $2p$ density. Hence the amount of covalent bonding has markedly increased in the higher oxides. This finding is consistent with XPS and UPS data.[68,75]

We have proposed that the here-predicted magnetic and insulator properties of U_3O_8 and Np_2O_5 could be tested by low-temperature resistivity and susceptibility measurements. Experimental investigations of the predicted valencies could provide further valuable information about the electronic structures.

ACKNOWLEDGMENTS

We thankfully acknowledge helpful discussions with D. Legut and R. Caciuffo. This work was supported by the Swedish Nuclear Materials Company (SKB), the Swedish Research Council (VR), STINT, and the Swedish National Infrastructure for Computing (SNIC).

*Present address: Laboratory of Reactor Physics and Systems Behaviour, Paul Scherrer Institut, CH-5232 Villigen PSI, Switzerland.
†Present address: CCSE, Japan Atomic Energy Agency, 6-9-3 Higashi-Ueno, Taito-ku, Tokyo 110-0015, Japan.

[1] J. Verbist, J. Riga, J. J. Pireaux, and R. Caudano, J. Electron Spectrosc. Relat. Phenom. **5**, 193 (1974).
[2] Y. Baer and J. Schoenes, Solid State Commun. **33**, 885 (1980).
[3] L. E. Cox, J. Electron Spectrosc. Relat. Phenom. **26**, 167 (1982).
[4] S. L. Dudarev, D. Nguyen Manh, and A. P. Sutton, Philos. Mag. B **75**, 613 (1997).
[5] S. L. Dudarev, G. A. Botton, S. Y. Savrasov, C. J. Humphreys, and A. P. Sutton, Phys. Rev. B **57**, 1505 (1998).
[6] S. L. Dudarev, G. A. Botton, S. Y. Savrasov, Z. Szotek, W. M. Temmerman, and A. P. Sutton, Phys. Status Solidi **166**, 429 (1998).
[7] K. N. Kudin, G. E. Scuseria, and R. L. Martin, Phys. Rev. Lett. **89**, 266402 (2002).
[8] R. Laskowski, G. K. H. Madsen, P. Blaha, and K. Schwarz, Phys. Rev. B **69**, 140408(R) (2004).
[9] Y. Yun, H. Kim, H. Kim, and K. Park, Nucl. Eng. Tech. **37**, 293 (2005).
[10] I. D. Prodan, G. E. Scuseria, and R. L. Martin, Phys. Rev. B **73**, 045104 (2006).
[11] Y. Yun, H. Kim, H. Lim, and K. Park, J. Korean Phys. Soc. **50**, 1285 (2007).
[12] B. Dorado, B. Amadon, M. Freyss, and M. Bertolus, Phys. Rev. B **79**, 235125 (2009).
[13] L. Petit, A. Svane, Z. Szotek, W. M. Temmerman, and G. M. Stocks, Phys. Rev. B **81**, 045108 (2010).
[14] O. Sakai, R. Shiina, and H. Shiba, J. Phys. Soc. Jpn. **74**, 457 (2005).
[15] Y. Tokunaga, Y. Homma, S. Kambe, D. Aoki, H. Sakai, E. Yamamoto, A. Nakamura, Y. Shiokawa, R. E. Walstedt, and H. Yasuoka, Phys. Rev. Lett. **94**, 137209 (2005).
[16] K. Kubo and T. Hotta, Phys. Rev. B **72**, 144401 (2005).
[17] P. Santini, S. Carretta, N. Magnani, G. Amoretti, and R. Caciuffo, Phys. Rev. Lett. **97**, 207203 (2006).
[18] L. Lynds, J. Inorg. Nucl. Chem. **24**, 1007 (1962).
[19] A. P. Cracknell and M. R. Daniel, Proc. Phys. Soc. **9**, 705 (1967).
[20] J. Faber, G. H. Lander, and B. R. Cooper, Phys. Rev. Lett. **35**, 1770 (1975).
[21] A. K. Burrell, T. M. McCleskey, P. Shulkla, H. Wang, T. Durakiewicz, D. P. Moore, C. G. Olson, J. J. Joyce, and Quanxi Jia, Adv. Mater. **19**, 3559 (2007).
[22] B. O. Loopstra, Acta Crystallogr. **17**, 651 (1964).
[23] B. O. Loopstra, J. Appl. Crystallogr. **3**, 94 (1970).
[24] S. Aronson, R. B. Roof, Jr., and J. Belle, J. Chem. Phys. **27**, 137 (1957).
[25] G. C. Allen, P. A. Tempest, and J. W. Tyler, Philos. Mag. B **54**, L67 (1986).
[26] R. G. J. Ball and R. W. Grimes, Philos. Mag. A **66**, 473 (1992).
[27] G. Rousseau, L. Desgranges, F. Charlot, N. Millot, J. C. Niépce, M. Pijolat, F. Valdivieso, G. Baldinozzi, and J. F. Bérar, J. Nucl. Mater. **355**, 10 (2006).
[28] R. G. J. Ball and P. G. Dickens, J. Mater. Chem. **1**, 105 (1991).
[29] R. J. McEachern and P. Taylor, J. Nucl. Mater. **254**, 87 (1998).
[30] L. E. Herranz and F. Feria, Prog. Nucl. Energy **51**, 201 (2009).
[31] J. J. Pireaux, J. Riga, E. Thibaut, C. Tenret-Noël, R. Caudano, and J. J. Verbist, Chem. Phys. **22**, 113 (1977).

[32]G. C. Allen, P. M. Tucker, and J. W. Tyler, Vacuum **32**, 481 (1982).
[33]M. Magnuson, S. M. Butorin, L. Werme, J. Nordgren, K. E. Ivanov, J.-H. Guo, and D. K. Shuh, Appl. Surf. Sci. **252**, 5615 (2006).
[34]G. C. Allen, A. J. Griffiths, and W. Suckling, Chem. Phys. Lett. **53**, 309 (1978).
[35]T. Z. Forbes, P. C. Burns, S. Skanthakumar, and L. Soderholm, J. Am. Chem. Soc. **129**, 2760 (2007).
[36]C. J. Pickard, B. Winkler, R. K. Chen, M. C. Payne, M. H. Lee, J. S. Lin, J. A. White, V. Milman, and D. Vanderbilt, Phys. Rev. Lett. **85**, 5122 (2000).
[37]H. R. Hoekstra, S. Siegel, L. H. Fuchs, and J. J. Katz, J. Phys. Chem. **59**, 136 (1955).
[38]L. Petit, A. Svane, Z. Szotek, and W. M. Temmerman, Science **301**, 498 (2003).
[39]P. A. Korzhavyi, L. Vitos, D. A. Andersson, and B. Johansson, Nature Mater. **3**, 225 (2004).
[40]D. A. Andersson, J. Lezama, B. P. Uberuaga, C. Deo, and S. D. Conradson, Phys. Rev. B **79**, 024110 (2009).
[41]D. A. Andersson, T. Watanabe, C. Deo, and B. P. Uberuaga, Phys. Rev. B **80**, 060101(R) (2009).
[42]G. Kresse and J. Hafner, Phys. Rev. B **47**, R558 (1993).
[43]G. Kresse and J. Furthmüller, Phys. Rev. B **54**, 11169 (1996).
[44]P. Blaha, K. Schwarz, G. K. H. Madsen, D. Kvasnicka, and J. Luitz, 2001 WIEN2K, Vienna University of Technology (ISBN 3-9501031-1-2).
[45]J. P. Perdew, in *Electronic Structure of Solids '91*, edited by P. Ziesche and H. Eschrig (Akademie Verlag, Berlin, 1991); J. P. Perdew, J. A. Chevary, S. H. Vosko, K. A. Jackson, M. R. Pederson, D. J. Singh, and C. Fiolhais, Phys. Rev. B **46**, 6671 (1992).
[46]R. Laskowski, G. K. H. Madsen, P. Blaha, and K. Schwarz, Phys. Rev. B **69**, 140408(R) (2004).
[47]J. P. Perdew, K. Burke, and M. Ernzerhof, Phys. Rev. Lett. **77**, 3865 (1996).
[48]J. P. Perdew and Y. Wang, Phys. Rev. B **45**, 13244 (1992).
[49]M. T. Czyzyk and G. A. Sawatzky, Phys. Rev. B **49**, 14211 (1994).
[50]V. I. Anisimov, I. V. Solovyev, M. A. Korotin, M. T. Czyzyk, and G. A. Sawatzky, Phys. Rev. B **48**, 16929 (1993).
[51]A. B. Shick, A. I. Liechtenstein, and W. E. Pickett, Phys. Rev. B **60**, 10763 (1999).
[52]J. Kuneš, P. Novák, M. Diviš, and P. M. Oppeneer, Phys. Rev. B **63**, 205111 (2001).
[53]J. Kuneš, P. Novák, R. Schmid, P. Blaha, and K. Schwarz, Phys. Rev. B **64**, 153102 (2001).
[54]J. A. Paixão, C. Detlefs, M. J. Longfield, R. Caciuffo, P. Santini, N. Bernhoeft, J. Rebizant, and G. H. Lander, Phys. Rev. Lett. **89**, 187202 (2002).
[55]R. Caciuffo, J. A. Paixão, C. Detlefs, M. J. Longfield, P. Santini, N. Bernhoeft, J. Rebizant, and G. H. Lander, J. Phys.: Condens. Matter **15**, S2287 (2003).
[56]See [http://www.webelements.com].
[57]R. Engmann and P. M. de Wolff, Acta Crystallogr. **16**, 993 (1963).
[58]C. Greaves and B. E. F. Fender, Acta Crystallogr. B **28**, 3609 (1972).
[59]M. Idiri, T. Le Bihan, S. Heathman, and J. Rebizant, Phys. Rev. B **70**, 014113 (2004).
[60]U. Benedict, S. Dabos, C. Dufour, and J. C. Spirlet, J. Less-Common Met. **121**, 461 (1986).
[61]The PAW radii that were used in the calculations are 1.561, 1.559, and 0.820 Å, for U, Np, and O, respectively.
[62]J. Faber and G. H. Lander, Phys. Rev. B **14**, 1151 (1976).
[63]R. Caciuffo, G. Amoretti, J. M. Fournier, A. Blaise, R. Osborn, A. D. Taylor, J. Larroque, and M. T. Hutchings, Solid State Commun. **79**, 197 (1991).
[64]P. Erdös, G. Solt, Z. Zolnierek, A. Blaise, and J. M. Fournier, Physica B **102**, 164 (1980).
[65]B.-T. Wang, H. Shi, W. Li, and P. Zhang, Phys. Rev. B **81**, 045119 (2010).
[66]R. Caciuffo (private communication).
[67]J. Schoenes, Phys. Rep. **63**, 301 (1980).
[68]B. W. Veal and D. J. Lam, Phys. Lett. A **49**, 466 (1974).
[69]P. M. Almond, S. Skanthakumar, L. Soderholm, and P. C. Burns, Chem. Mater. **19**, 280 (2007).
[70]T. Z. Forbes, P. C. Burns, L. Soderholm, and S. Skanthakumar, Chem. Mater. **18**, 1643 (2006).
[71]T. Nakamoto, M. Nakada, A. Nakamura, Y. Haga, and Y. Ōnuki, Solid State Commun. **109**, 77 (1999).
[72]T. Nakamoto, M. Nakada, and A. Nakamura, J. Nucl. Sci. Technol. (Suppl.) **3**, 102 (2002).
[73]P. M. Almond, R. E. Sykora, S. Skanthakumar, L. Soderholm, and T. E. Albrecht-Schmitt, Inorg. Chem. **43**, 958 (2004).
[74]M.-T. Suzuki, N. Magnani, and P. M. Oppeneer, Phys. Rev. B **82**, 241103(R) (2010).
[75]A. Seibert, T. Gouder, and F. Huber, J. Nucl. Mater. **389**, 470 (2009).
[76]J. M. Haschke and T. H. Allen, J. Alloys Compd. **336**, 124 (2002).